Armbrusterite, $K_5Na_6Mn^{3+}Mn^{2+}_{14}[Si_9O_{22}]_4(OH)_{10}\cdot4H_2O$, a new Mn hydrous heterophyllosilicate from the Khibiny alkaline massif, Kola Peninsula, Russia

VICTOR N. YAKOVENCHUK,[1] SERGEY V. KRIVOVICHEV,[2,*] YAKOV A. PAKHOMOVSKY,[1]
GREGORY YU. IVANYUK,[1] EKATERINA A. SELIVANOVA,[1] YURY P. MEN'SHIKOV,[1]
AND SERGEY N. BRITVIN[2]

[1]Geological Institute of the Kola Science Center of the Russian Academy of Sciences, 14 Fersman Str., Apatity 184209, Murmansk Region, Russia
[2]St. Petersburg State University, Department of Crystallography, University Emb. 7/9 St. Petersburg 199034, Russia

ABSTRACT

Armbrusterite, ideally $K_5Na_6Mn^{3+}Mn^{2+}_{14}[Si_9O_{22}]_4(OH)_{10}\cdot4H_2O$, is a new silicate of potassium, sodium, and manganese found in a thin cancrinite-aegirine-microcline vein within urtite at Mt. Kukisvumchorr. The mineral occurs in intimate association with raite. Other associated minerals are lamprophyllite, mangan-neptunite, pectolite, vinogradovite, calcite, molybdenite, galena, sphalerite, and fluorite. Armbrusterite occurs as split, curved crystals and spherulites ($\leq$2 mm diameter). The mineral is translucent (transparent in thin fragments), dark reddish-brown. It has vitreous luster and light-brown streak. Cleavage is perfect on (001) and the fracture is uneven. Mohs hardness is about 3.5. In transmitted light, the mineral is reddish-brown, with strong pleochroism: X = light yellowish-brown, Y and Z = dark reddish-brown; dispersion $r > v$, weak. Armbrusterite is biaxial (–): α = 1.532(2), β = 1.560(2), γ = 1.564(2) (for λ = 589 nm), $2V$ varies from 10° to 20°. Optical orientation: X is perpendicular to (001). The mean chemical composition determined by electron microprobe and the Penfield method (for H_2O) is (wt%): Na_2O 5.26, MgO 0.19, Al_2O_3 0.04, SiO_2 56.02, K_2O 6.13, CaO 0.26, TiO_2 0.04, MnO 23.62, Mn_2O_3 2.07, FeO 0.65, ZnO 0.20, H_2O 4.1, sum. 98.58. Empirical formula calculated on the basis of Si = 36 is $K_{5.03}Na_{6.55}(Mn^{2+}_{12.86}Mn^{3+}_{1.01}Fe^{2+}_{0.35}Mg_{0.18}Ca_{0.18}Zn_{0.09}Al_{0.03}Ti_{0.02})_{\Sigma=14.72}[Si_{36}O_{88}](OH)_{10.10}\cdot3.75\ H_2O$. Armbrusterite is monoclinic, $C2/m$, a = 17.333(2), b = 23.539(3), c = 13.4895(17) Å, β = 115.069(9)°, V = 4985.4(11) Å^3, Z = 2. The strongest X-ray powder-diffraction lines are [d in Å, (I), (hkl)]: 12.28 (100) (001), 4.10 (10) (003), 3.562 (10) (113, 261), 3.260 (18) (114), 3.117 (13) (203), 3.077 (54) (004), 2.622 (10) (371). The crystal structure of armbrusterite was refined to R_1 = 0.085 on the basis of 3960 unique observed reflections. The structure is based upon double silicate $[Si_9O_{22}]$ layers consisting of 5-, 6-, 7-, and 8-membered tetrahedra rings. The layers are linked via octahedral sheets formed by Na and Mn octahedra. The interior of the double silicate layers is occupied by K^+ cations and H_2O molecules. The mineral is named in honor of Thomas Armbruster (b. 1950; University of Berne) for his outstanding contribution to structural mineralogy and crystallography, especially to the study of Mn-rich minerals.

Keywords: Armbrusterite, new mineral, sodium-potassium-manganese silicate, crystal structure, Khibiny massif, Kola Peninsula

INTRODUCTION

Hydrous manganese silicates represent an interesting class of phyllosilicate minerals (Liebau 1985; Guggenheim and Eggleton 1987, 1988; Hughes et al. 2003; Krivovichev et al. 2004). One of the most distinguishing structural features is the existence of complex types of silicate anions that result from inversion and tilting of silicate tetrahedra. Here we report the occurrence and crystal structure of armbrusterite, a new Mn silicate that contains a novel type of silicate anion of unusual complexity.

Armbrusterite was found in the Khibiny massif, Kola Peninsula, Russia. The genesis of Mn minerals differs between alkaline massifs of the Kola Peninsula. In particular, Mn minerals are uncommon in the Khibiny massif, whereas they are more abun-dant in the Lovozero massif. In Khibiny, Mn-dominant eudialyte, mangan-neptunite, and låvenite-normandite are primary minerals in foyaite, ijolite-urtite, and pegmatite veins. Other Mn minerals such as the labuntsovite-group minerals, manaksite, kupletskite, shafranovskite, tisinalite, zakharovite, raite, etc. occur as a result of Mn redistribution during secondary hydrothermal alteration of initial phases (Yakovenchuk et al. 2005).

In 1987, A.S. Podlesny discovered a cancrinite-aegirine-microcline vein within ijolite-urtite at Mt. Kukisvumchorr (Kirov Mine, horizon + 252 m). He provided the first author with specimens for investigation. Electron microprobe analysis and powder X-ray diffraction indicated the presence of raite in intimate intergrowths with an unknown K, Na, and Mn silicate. At that time, we were unable to find sufficient material for a single-crystal X-ray structure study. In 2004, further review of these specimens revealed a single crystal of good quality, which

* E-mail: skrivovi@mail.ru

allowed complete characterization of this mineral.

The mineral is named in honor of Thomas Armbruster (b. 1950), Laboratory of Chemical and Mineralogical Crystallography, University of Berne, for his outstanding contribution to structural mineralogy and crystallography, especially to the study of Mn silicates (Armbruster et al. 1993a, 1993b, 2001, 2002, etc.). Both the mineral and mineral name have been approved by the Commission on New Minerals and Mineral Names of the International Mineralogical Association (proposal 2005-035). The holotype specimens of armbrusterite were deposited in the Geological and Mineralogical Museum of the Geological Institute of the Kola Science Centre, Russian Academy of Sciences (Apatity, Russia), registration number 6280; co-type material is deposited in the Mineralogical museum of St. Petersburg State University, Russia, registration number 1/19174.

OCCURRENCE

The deposit at Mt. Kukisvumchorr (Khibiny massif, Kola Peninsula, Russia) consists of large lens of apatite-nepheline rocks dipping northeast at 26° to 32° (Yakovenchuk et al. 2005). The lens is 40 m thick on the northern flank, ≤180 m thick to the south, and 1850 m long. The upper contact with feldspar-bearing ijolite-urtite, malignite, and rischorrite is marked by a thin zone of titanite-rich rock. Some 10–50 m below the main ore body there is the second, parallel, 5–30 m wide lens of apatite-nepheline rock. The deposit is accompanied by a major conical 0.2–2.5 m wide shear-zone which dips at an angle of about 45° to the center of the massif and is marked by gneissose apatite-nepheline rocks, brecciated zones, layers of ijolite, juvite, malignite, and also pegmatite and hydrothermal veins. Armbrusterite was found in a thin (≤10 cm wide and 2 m long) cancrinite-aegirine-microcline vein in ijolite-urtite overlying the apatite ore body (the Kirov Mine, horizon + 252 m).

Marginal parts of the vein consist of aegirine-microcline aggregate with lamprophyllite, sphalerite and galena inclusions. In interstices, there are mangan-neptunite and aegirine crystals of ≤4 mm long. The axial cancrinite zone of the vein contains numerous voids sometimes filled with calcite. Colorless natrolite crystals (≤3 mm long), white lamellar pectolite (≤3 cm long), acicular vinogradovite aggregates (≤2 mm long) and lamellar molybdenite segregations (≤1 cm diameter) grow on gray cancrinite crystals (≤1 cm long) in voids. Dark reddish-brown aggregates of armbrusterite (sometimes in intimate intergrowth with dark-brown fibrous raite) have crystallized on microcline, cancrinite and pectolite crystals or form inclusions in calcite. The last phases in this association are solid organics which cover all of the earlier minerals in voids.

PHYSICAL AND OPTICAL PROPERTIES

Armbrusterite forms poorly shaped split and curved crystals (≤1 mm long) as well as clusters (≤8 mm diameter) of spherulites (≤2 mm diameter) consisting of platy crystals (Fig. 1). No twinning was observed. Macroscopically, armbrusterite is dark reddish-brown with a vitreous luster. The mineral is translucent in aggregates and transparent in thin lamellae. The streak is light brown. Cleavage is perfect on (001). Armbrusterite is brittle and has uneven fracture. Mohs hardness is about 3.5. The density as determined by the float and sink method in Clerici solution is
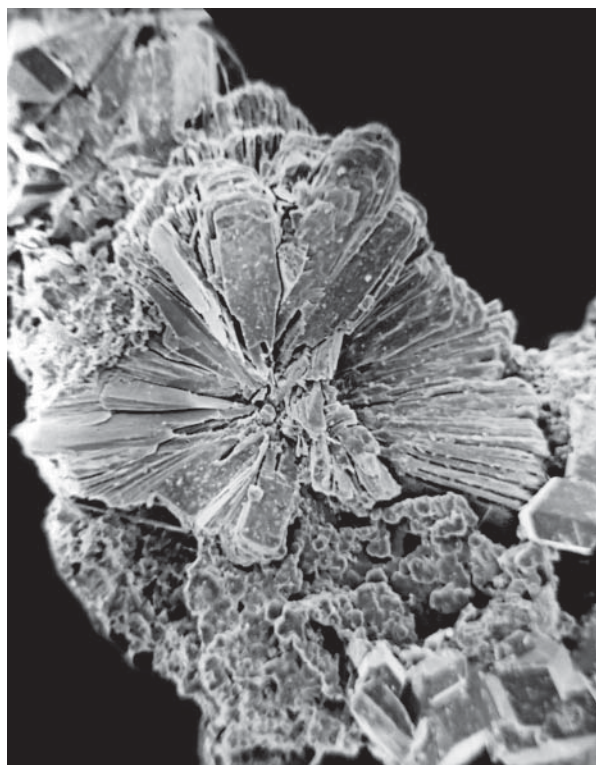

FIGURE 1. Spherulite of platy crystals of armbrusterite (2 mm diameter) on cancrinite and calcite.

2.78(2) g/cm^3; density calculated on the basis of the empirical formula and powder data is 2.579 g/cm^3. The apparent difference in measured and calculated densities might be explained by partial incorporation of Ti+ ions from Clerici solution into the porous structure of armbrusterite.

Armbrusterite is biaxial (–): $\alpha = 1.532(2)$, $\beta = 1.560(2)$, $\gamma = 1.564(2)$ (for $\lambda = 589$ nm), $2V_{meas} = 10–20°$, $2V_{calc} = 41°$. Optical orientation: X is perpendicular to (001). In transmitted light, the mineral is reddish-brown, with a strong pleochroism: X = light yellowish-brown, Y and Z = dark reddish-brown; dispersion $r > v$, weak. The Gladstone-Dale relationship provides a compatibility index of –0.043 (with single-crystal data and $D_{calc.}$), 0.044 (with single-crystal data and $D_{meas.}$), and estimated to be good, and of 0.026 (with powder data and $D_{calc.}$), estimated to be excellent (Mandarino 1981).

CHEMICAL COMPOSITION

Chemical composition of armbrusterite was studied by wavelength dispersive spectrometry using a Cameca MS-46 electron microprobe (Geological Institute, Kola Science Centre of the Russian Academy of Sciences, Apatity) operating at 20 kV and 20–30 nA and a 5 μm beam diameter. The following standards were used: lorenzenite (for Na, Ti), pyrope (Mg, Al), diopside (Si, Ca), wadeite (K), synthetic MnCO$_3$ (Mn), hematite (Fe), and sphalerite (Zn). Water content was determined by the Penfield method for purified material. Table 1 provides the analytical results for four different spherulites; each analysis is the average of 6–10 points.

The mean composition of armbrusterite corresponds to the

empirical formula (calculated on the basis of Si = 36 atoms per formula units, apfu): $K_{5.03}Na_{6.55}(Mn^{2+}_{12.86}Mn^{3+}_{1.01}Fe^{2+}_{0.35}Mg_{0.18}Ca_{0.18}Zn_{0.09}Al_{0.03}Ti_{0.02})_{\Sigma=14.72}[Si_{36}O_{88}](OH)_{10.10}\cdot3.75\ H_2O$. Simplified formula calculated on the basis of crystal-structure analysis is $K_5Na_6Mn^{3+}Mn^{2+}_{14}[Si_9O_{22}]_4(OH)_{10}\cdot4H_2O$, which would require oxide weight percentages K_2O 6.16, Na_2O 4.87, MnO 26.01, Mn_2O_3 2.07, SiO_2 56.65, H_2O 4.24, total 100.00 wt%.

CRYSTAL STRUCTURE

Experimental Methods

The crystal of armbrusterite selected for data collection was mounted on a glass fiber. Data were collected by means of a STOE IPDS diffractometer in the Institute of Mineralogy and Petrology, University of Innsbruck, using monochromated Mo$K\alpha$ radiation and frame widths of 0.3° in ω up to θ = 27.5°. The unit-cell dimensions (Table 2) were refined by least-squares techniques. The data were corrected for Lorentz, polarization, absorption, and background effects. The intensity statistics indicated space group $C2/m$. The structure was solved and refined by means of the program SHELX-97. Refinement of atom position and displacement parameters and the inclusion of a refinable weighting scheme of the structure factors resulted in final agreement index (R_1) of 0.085, calculated for the 3960 unique observed reflections ($|F_o| > 4\sigma F$). The final atomic parameters and bond-valence sums are listed in Table 3. Selected interatomic distances are given in Table 4.

RESULTS

The structure of armbrusterite contains six octahedrally coordinated sites, which can be assigned to Mn according to the site-scattering factor. The Mn1, Mn2, Mn3, Mn4, and Mn6 positions have corresponding average <Mn-O> bond lengths in

TABLE 1. Chemical composition of armbrusterite (wt%)

	1	2	3	4	Mean
Na₂O	5.33	5.30	5.33	5.07	5.26 ± 0.13
MgO	0.27	0.15	0.10	0.24	0.19 ± 0.08
Al₂O₃	0.08	n.d.	n.d.	0.09	0.04 ± 0.05
SiO₂	54.28	57.13	57.14	55.51	56.02 ± 1.38
K₂O	6.55	7.92	5.72	4.32	6.13 ± 1.51
CaO	0.37	0.32	0.15	0.20	0.26 ± 0.10
TiO₂	0.06	n.d.	0.08	n.d.	0.04 ± 0.04
MnO	22.95	24.86	22.57	24.09	23.62 ± 1.05
Mn₂O₃	2.07	2.07	2.07	2.07	2.07*
FeO	0.37	0.35	1.49	0.39	0.65 ± 0.56
ZnO	0.28	0.29	n.d.	0.21	0.20 ± 0.13
H₂O					4.10
Total	92.61	98.39	94.65	92.19	98.58

* Calculated on the basis of ideal formula (1Mn³⁺ apfu).

TABLE 2. Crystallographic data and refined parameters for armbrusterite

a (Å)	17.333(2)
b (Å)	23.539(3)
c (Å)	13.4895(17)
β (°)	115.069(9)
V (Å³)	4985.4(11)
Space group	$C2/m$
Z	2
D_{calc} (g/cm³)	2.53
Crystal size (mm)	0.22 × 0.16 × 0.04
Radiation	Mo$K\alpha$
Total Ref.	18553
Unique Ref.	5414
Unique $|F_o| \geq 4\sigma_F$	3960
R_1	0.086
wR_2	0.212
S	1.069

Notes: $R1 = \Sigma||F_o| - |F_c||/\Sigma|F_o|$; $wR_2 = \{\Sigma[w(F_o^2 - F_c^2)^2]/\Sigma[w(F_o^2)^2]\}^{1/2}$; $w = 1/[\Sigma^2(F_o^2) + (aP)^2 + bP]$, where $P = (F_o^2 + 2F_c^2)/3$; $s = \{\Sigma[w(F_o^2 - F_c^2)]/(n - p)\}^{1/2}$ where n is the number of reflections and p is the number of refined parameters.

the range of 2.20–2.23 Å. Their bond-valence sums range from 1.80 to 2.02 v.u. (valence units), in good agreement with 2+ formal charge. In contrast, the coordination of the Mn5 site is relatively compressed: its average <Mn5-O> bond length equals 2.04 Å. Bond-valence calculations on the basis of the Mn^{2+}-O and Mn^{3+}-O curves provided by Brese and O'Keeffe (1991) result in the bond-valence sum of 3.10 and 2.86 v.u., respectively. This corresponds to the occupation of this site by the Mn^{3+} rather than Mn^{2+} cations. We believe that this site may host Fe^{2+} (as much as 35%, according to the chemical analyses) or high-valent cations such as Ti^{4+} and Al^{3+} which were detected by electron microprobe analysis. The latter hypothesis may explain the apparent absence of Jahn-Teller distortions at this site that one would expect for the Mn^{3+} cation (Armbruster et al. 1993a, 1993b). Another explanation would be that the Jahn-Teller distortion has a local character and the observed apparent undistorted environment is an averaged position. However, analysis of displacement parameters using the THMA11 (Thermal Motion Analysis) code (Dunitz et al. 1988) did not reveal any peculiarities in mean-square-displacement amplitudes between the Mn5 site and the coordinating OH2 and O10 anions. Thus, the apparent absence of Jahn-Teller distortion is either due to the other cation substitutions or due to some complicated bond valence vs. bond topology requirements at this site. There are two symmetrically independent Na sites, each of which is octahedrally coordinated. The structure contains nine Si^{4+} positions with characteristic Si-O bond lengths.

Figure 2 shows projection of the structure of armbrusterite along the b axis. The structure is based upon double silicate layers with the composition of $[Si_9O_{22}]^{8-}$ separated by sheets of MnO_6 and NaO_6 octahedra. The single silicate sheet is shown in Figure 3a. This appears to be the first example of a two-dimensional (planar sheet) silicate anion that consists of 5-, 6-, 7-, and 8-membered tetrahedral rings (see below). Eight of nine symmetrically independent SiO_4 tetrahedra have their non-shared corners oriented towards the octahedral sheet, whereas one, $Si8O_4$, is oriented in the opposite direction and is responsible for linking two adjacent silicate sheets.

The MnO_6 octahedra within the octahedral sheet (Fig. 3b) comprise a "dioctahedral" arrangement (if only Mn is considered) with Na^+ cations positioned in the remaining octahedral
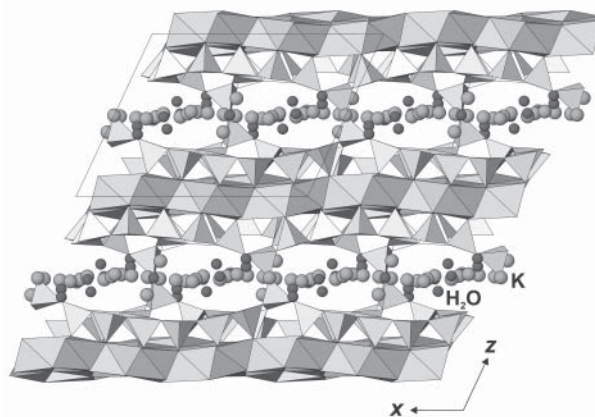

FIGURE 2. Crystal structure of armbrusterite in projection along the b axis.

TABLE 3. Atomic coordinates, displacement parameters ($Å^2$), and bond-valence sums* (*BVS, v.u.*) for armbrusterite

Atom	s.o.f. ‡	x	y	z	U_{eq}	BVS*
Mn1	1	0	0.06931(8)	0	0.0223(4)	2.02
Mn2	1	0	0.21062(8)	0	0.0219(4)	1.88
Mn3	1	0.32397(8)	0.07102(5)	0.96233(12)	0.0223(3)	1.94
Mn4	1	0.84790(11)	0	0.04652(17)	0.0229(4)	1.80
Mn5	1	½	0	0	0.0214(6)	3.10
Mn6	1	0.67138(8)	0.78453(6)	0.01290(12)	0.0230(3)	1.92
Na1	1	0.8465(2)	0.14408(15)	0.0470(3)	0.0294(8)	1.02
Na2	1	½	0.8511(2)	0	0.031(1)	1.14
Si1	1	0.28669(14)	0.06392(10)	0.1804(2)	0.0203(5)	4.20
Si2	1	0.85334(14)	0.86802(10)	0.7929(2)	0.0205(5)	4.11
Si3	1	0.39902(14)	0.06387(10)	0.7713(2)	0.0213(5)	3.97
Si4	1	0.85790(15)	0.74466(10)	0.7667(2)	0.0222(5)	4.01
Si5	1	0.01462(15)	0.06473(9)	0.2525(2)	0.0206(5)	3.98
Si6	1	0.02831(15)	0.75457(10)	0.7661(2)	0.0221(5)	4.07
Si7	1	0.25042(14)	0.85840(10)	0.7343(2)	0.0209(5)	3.93
Si8	1	0.05700(14)	0.14539(10)	0.6269(2)	0.0206(5)	4.23
Si9	1	0.43999(14)	0.13157(10)	0.2007(2)	0.0201(5)	4.00
OH1	1	0.2409(6)	0	0.8736(8)	0.0265(19)	0.97
OH2	1	0.4119(6)	0	0.0649(8)	0.029(2)	1.01
O3	1	0.2454(4)	0.0672(2)	0.0507(5)	0.0234(13)	1.97
OH4	1	0.0899(6)	0	0.0692(8)	0.027(2)	1.13
O5	1	0.4031(4)	0.1383(2)	0.0717(5)	0.0243(14)	2.01
O6	1	0.2603(4)	0.8580(3)	0.8579(5)	0.0269(14)	1.72
O7	1	0.9042(4)	0.7291(3)	0.8946(5)	0.0250(13)	1.88
O8	1	0.9465(4)	0.0659(2)	0.1274(5)	0.0238(13)	1.83
O9	1	0.9156(4)	0.8623(2)	0.9180(5)	0.0231(13)	1.99
O10	1	0.4251(4)	0.0613(3)	0.8999(5)	0.0242(13)	2.04
O11	1	0.0479(5)	0	0.2970(8)	0.0255(19)	1.86
O12	1	0.9007(4)	0.8973(3)	0.7236(5)	0.0271(14)	1.95
O13	1	0.8129(4)	0.8070(2)	0.7384(5)	0.0237(13)	1.97
O14	1	0.4644(4)	0.1037(3)	0.7424(5)	0.0244(13)	1.92
O15	1	0.0671(4)	0.7719(3)	0.8922(5)	0.0259(14)	1.84
O16	1	0.0597(4)	0.6928(3)	0.7419(5)	0.0236(13)	1.95
O17	1	0.3033(4)	0.9103(3)	0.7082(5)	0.0245(13)	1.91
O18	1	0	0.1576(4)	½	0.032(2)	2.14
O19	1	0.7830(4)	0.7004(3)	0.6985(5)	0.0252(13)	1.98
O20	1	0.2999(6)	0	0.2285(8)	0.027(2)	2.04
O21	1	0.1529(4)	0.1329(3)	0.6433(6)	0.0274(14)	2.03
O22	1	0.0547(4)	0.1999(3)	0.6958(6)	0.0315(15)	2.09
O23	1	0.3814(4)	0.0906(3)	0.2391(5)	0.0290(15)	1.99
O24	1	0.3989(5)	0	0.7223(7)	0.0238(18)	1.90
OH25	1	0.7508(4)	0.7120(3)	0.0734(6)	0.0270(14)	1.00
O26	1	0.9254(4)	0.7478(3)	0.7106(5)	0.0284(14)	1.95
O27	1	0.7697(4)	0.9067(3)	0.7654(5)	0.0293(15)	2.07
O28	1	0.9767(4)	0.0893(3)	0.3356(6)	0.0284(15)	2.03
K1	0.30	0.210(1)	0.9513(7)	0.4905(13)	0.090(4)	
K2	0.28	0.505(1)	0.0000	0.6035(16)	0.072(5)	
K3	0.16	0.0000	0.0000	0.5000	0.042(7)	
K5	0.20	0.9725(14)	0.6967(11)	0.495(2)	0.100†	
K6	0.17	0.815(2)	0.6705(14)	0.490(3)	0.100†	
K7	0.17	0.854(2)	0.7263(14)	0.479(3)	0.100†	
K10	0.11	0.824(3)	0.560(2)	0.477(4)	0.100†	
K11	0.12	0.398(3)	0.0665(18)	0.485(4)	0.100†	
H_2O1	0.35	0.0000	0.652(3)	0.5000	0.100†	
H_2O2	0.34	0.0000	0.586(3)	0.5000	0.100†	
H_2O3	0.26	0.878(3)	0.683(2)	0.434(4)	0.100†	
H_2O4	0.29	0.824(3)	0.613(2)	0.478(4)	0.100†	
H_2O5	0.26	0.243(4)	0.0000	0.413(5)	0.100†	
H_2O6	0.26	0.218(4)	0.0000	0.509(5)	0.100†	
H_2O7	0.70	0.8609(14)	0.0000	0.3821(18)	0.100†	

* Calculated for octahedral-tetrahedral framework using bond-valence parameters from Brese and O'Keeffe (1991); contributions from hydrogen bonds and disordered K^+ cations are not taken into account.
† Fixed during refinement.
‡ s.o.f. = site occupation factor.

sites. The occupancy of both Mn^{2+} and Na^+ cations in the sheet is also observed in the structure of shafranovskite (Krivovichev et al. 2004).

Together with the octahedral sheets, silicate double layers form a mixed octahedral-tetrahedral framework (i.e., approximating a 2:1 layer) which is typical for the hydrous Mn phyllosilicates (Guggenheim and Eggleton 1987, 1988; Hughes et al. 2003). The interior of the double silicate layers (i.e., the interlayer region of an ideal 2:1 layer phyllosilicate) is occupied by disordered K^+ cations and H_2O molecules.

POWDER X-RAY DIFFRACTION PATTERN

The powder X-ray diffraction pattern of armbrusterite was obtained by means of a DRON-2 diffractometer operating at 40 kV and 25 mA with monochromatized Cu$K\alpha$ radiation. Table 5 provides a comparison of the observed and calculated powder

TABLE 3. —*Extended.*

| Atom	U_{11}	U_{22}	U_{33}	U_{23}	U_{13}	U_{12}
Mn1	0.0162(8)	0.0150(9)	0.0381(11)	0	0.0139(8)	0
Mn2	0.0153(8)	0.0170(9)	0.0355(11)	0	0.0127(8)	0
Mn3	0.0168(6)	0.0157(7)	0.0388(8)	−0.0005(5)	0.0160(6)	−0.0003(5)
Mn4	0.0155(8)	0.0178(9)	0.0380(11)	0	0.0141(8)	0
Mn5	0.0137(11)	0.0181(13)	0.0351(15)	0	0.0129(11)	0
Mn6	0.0174(6)	0.0173(7)	0.0395(8)	0.0011(5)	0.0170(6)	0.0008(5)
Na1	0.0225(18)	0.0192(18)	0.047(2)	0.001(2)	0.0151(17)	−0.0010(14)
Na2	0.026(3)	0.026(3)	0.048(3)	0	0.024(2)	0
Si1	0.0150(10)	0.0156(11)	0.0345(14)	0.0009(9)	0.0144(10)	−0.0001(8)
Si2	0.0135(10)	0.0166(11)	0.0342(13)	−0.0003(9)	0.0128(10)	0.0018(8)
Si3	0.0138(10)	0.0181(12)	0.0354(14)	0.0000(9)	0.0139(10)	−0.0004(8)
Si4	0.0148(10)	0.0186(12)	0.0346(14)	−0.0010(9)	0.0117(10)	−0.0014(9)
Si5	0.0167(11)	0.0133(11)	0.0363(14)	0.0000(9)	0.0156(10)	0.0009(8)
Si6	0.0165(11)	0.0180(12)	0.0359(14)	0.0008(9)	0.0151(10)	−0.0014(9)
Si7	0.0130(10)	0.0170(11)	0.0340(13)	0.0006(9)	0.0113(10)	0.0005(8)
Si8	0.0125(10)	0.0198(12)	0.0319(13)	−0.0015(9)	0.0117(10)	−0.0001(8)
Si9	0.0124(10)	0.0150(11)	0.0354(13)	−0.0004(9)	0.0124(10)	−0.0013(8)
OH1	0.023(4)	0.022(5)	0.040(5)	0	0.018(4)	0
OH2	0.021(4)	0.023(5)	0.049(6)	0	0.019(4)	0
O3	0.018(3)	0.016(3)	0.041(4)	−0.001(2)	0.016(3)	−0.001(2)
OH4	0.024(4)	0.022(5)	0.038(5)	0	0.016(4)	0
O5	0.016(3)	0.018(3)	0.038(4)	−0.003(2)	0.011(3)	0.002(2)
O6	0.022(3)	0.028(3)	0.032(4)	−0.002(3)	0.012(3)	−0.003(2)
O7	0.018(3)	0.027(3)	0.033(3)	−0.003(3)	0.014(3)	−0.004(2)
O8	0.022(3)	0.016(3)	0.037(4)	−0.004(2)	0.016(3)	−0.006(2)
O9	0.016(3)	0.018(3)	0.037(4)	0.001(2)	0.014(3)	−0.001(2)
O10	0.016(3)	0.022(3)	0.039(4)	−0.001(3)	0.017(3)	0.002(2)
O11	0.025(4)	0.014(4)	0.044(5)	0	0.021(4)	0
O12	0.026(3)	0.020(3)	0.040(4)	−0.003(3)	0.019(3)	−0.004(3)
O13	0.019(3)	0.012(3)	0.038(4)	0.000(2)	0.009(3)	−0.004(2)
O14	0.023(3)	0.017(3)	0.035(3)	0.001(3)	0.014(3)	−0.003(2)
O15	0.019(3)	0.028(3)	0.032(3)	−0.002(3)	0.012(3)	0.002(3)
O16	0.022(3)	0.021(3)	0.033(3)	0.003(3)	0.017(3)	0.002(2)
O17	0.015(3)	0.021(3)	0.041(4)	−0.001(3)	0.015(3)	−0.002(2)
O18	0.022(4)	0.040(6)	0.035(5)	0	0.013(4)	0
O19	0.018(3)	0.017(3)	0.039(4)	0.002(3)	0.011(3)	−0.004(2)
O20	0.031(5)	0.013(4)	0.039(5)	0	0.017(4)	0
O21	0.016(3)	0.030(4)	0.042(4)	−0.005(3)	0.017(3)	−0.001(2)
O22	0.030(3)	0.025(4)	0.044(4)	−0.005(3)	0.021(3)	0.002(3)
O23	0.018(3)	0.033(4)	0.035(4)	0.000(3)	0.010(3)	−0.010(3)
O24	0.023(4)	0.019(4)	0.037(5)	0	0.020(4)	0
OH25	0.018(3)	0.024(3)	0.042(4)	0.003(3)	0.016(3)	0.002(2)
O26	0.014(3)	0.038(4)	0.033(4)	−0.002(3)	0.010(3)	−0.004(3)
O27	0.022(3)	0.030(4)	0.035(4)	0.001(3)	0.012(3)	0.012(3)
O28	0.023(3)	0.022(3)	0.051(4)	−0.001(3)	0.027(3)	−0.004(3)
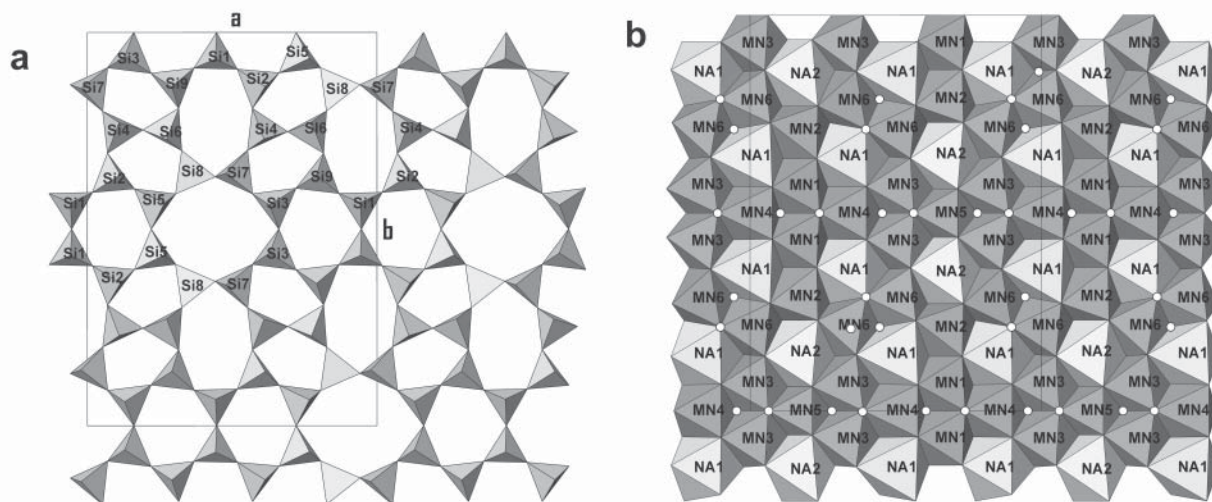
FIGURE 3. Projections of single tetrahedral (**a**) and octahedral (**b**) sheets of armbrusterite. White circles in **b** indicate positions of the OH sites.

patterns. The unit-cell parameters refined from the powder data are: $a = 17.34(5)$, $b = 23.50(5)$, $c = 13.57(3)$ Å, $\beta = 115.2(1)°$, $V = 5004.3(5)$ Å^3, $Z = 2$.

DISCUSSION

Armbrusterite is a new member of the group of modulated manganese phyllosilicates (Guggenheim and Eggleton 1987,

1988; Grice and Gault 1995; Hughes et al. 2003; Krivovichev et al. 2004, etc.). In many of these minerals, two-dimensional silicate anions have unique topologies induced by the incommensurate relationships between the octahedral and tetrahedral sheets (Liebau 1985; Guggenheim and Eggleton 1987, 1988). Table 6 provides list of selected (ideally 2:1 or 1:1 layers) Mn phyllosilicates, whereas Figure 4 shows two-dimensional graphs of tetrahedral sheets in pyrosmalite, parsettensite, varennesite, tamaite, bannisterite, and intersilite. Nodes symbolize Si centers, and an edge between two nodes corresponds to common O atoms between two corresponding SiO$_4$ tetrahedra (Liebau 1985; Krivovichev 2005). In Table 6, each graph is described by a ring symbol, i.e. a sequence $p_1^{r1}p_2^{r2} \dots p_n^{rn}$, where $p_1, p_2, \dots, p_n$ are numbers of nodes in a ring and r1, r2, ... rn are relative numbers of the corresponding rings in a graph.

Figures 5a and 5b show topologies of silicate anions in armbrusterite and bementite, respectively. By inspection of Figures 4 and 5, the bementite topology is most closely related to that of armbrusterite. Both graphs are constructed from double 6-mem-

TABLE 4. Selected bond lengths (Å) in the structure of armbrusterite

Mn1-O9	2.141(6) 2×	Si1-O3	1.587(7)
Mn1-OH4	2.174(6) 2×	Si1-O27	1.605(7)
Mn1-O8	2.274(6) 2×	Si1-O20	1.616(4)
<Mn1-O>	2.20	Si1-O23	1.617(6)
		<Si1-O>	1.61
Mn2-O7	2.189(6) 2×		
Mn2-O9	2.223(6) 2×	Si2-O9	1.577(7)
Mn2-O15	2.253(6) 2×	Si2-O27	1.617(6)
<Mn2-O>	2.22	Si2-O13	1.631(6)
		Si2-O12	1.634(7)
Mn3-O3	2.159(6)	<Si2-O>	1.61
Mn3-O6	2.163(6)		
Mn3-OH1	2.200(6)	Si3-O10	1.598(7)
Mn3-O5	2.203(6)	Si3-O17	1.628(6)
Mn3-O10	2.254(6)	Si3-O14	1.640(6)
Mn3-OH2	2.290(7)	Si3-O24	1.642(4)
<Mn3-O>	2.21	<Si3-O>	1.63
Mn4-OH1	2.222(9)	Si4-O7	1.607(7)
Mn4-O8	2.222(6) 2×	Si4-O19	1.614(6)
Mn4-OH4	2.242(10)	Si4-O13	1.629(6)
Mn4-O3	2.246(6) 2×	Si4-O26	1.642(7)
<Mn4-O>	2.23	<Si4-O>	1.62
Mn5-O10	2.026(6) 4×	Si5-O8	1.599(7)
Mn5-OH2	2.056(9) 2×	Si5-O28	1.626(7)
<Mn5-O>	2.04	Si5-O12	1.630(6)
		Si5-O11	1.650(4)
Mn6-OH25	2.125(7)	<Si5-O>	1.63
Mn6-OH25	2.126(6)		
Mn6-O7	2.182(6)	Si6-O15	1.593(7)
Mn6-O5	2.241(6)	Si6-O22	1.620(7)
Mn6-O15	2.277(6)	Si6-O26	1.624(6)
Mn6-O6	2.383(7)	Si6-O16	1.633(6)
<Mn6-O>	2.22	<Si6-O>	1.62
Na1-OH25	2.391(7)	Si7-O6	1.602(7)
Na1-O3	2.401(7)	Si7-O21	1.627(7)
Na1-O15	2.406(7)	Si7-O19	1.643(6)
Na1-O8	2.444(7)	Si7-O17	1.653(6)
Na1-O9	2.501(8)	<Si7-O>	1.63
Na1-O6	2.662(8)		
<Na1-O>	2.47	Si8-O22	1.595(7)
		Si8-O18	1.599(3)
Na2-O5	2.280(6) 2×	Si8-O21	1.609(6)
Na2-O10	2.505(8) 2×	Si8-O28	1.610(7)
Na2-O7	2.519(8) 2×	<Si8-O>	1.60
<Na2-O>	2.43		
		Si9-O5	1.587(7)
		Si9-O16	1.636(6)
		Si9-O23	1.636(7)
		Si9-O14	1.639(6)
		<Si9-O>	1.62

TABLE 5. X-ray powder diffraction data for armbrusterite

I	D_{obs}	D_{calc}	hkl
100	12.28	12.280	001
1	7.79	7.847	200
2	6.15	6.140	002
1	5.60	5.616, 5.613	201, $\bar{3}$11
1	5.44	5.442	022
1	5.31	5.300	041
1	5.13	5.106	310
2	4.65	4.651	$\bar{3}$31
4	4.32	4.349, 4.306	$\bar{3}$32, 401
6	4.24	4.245	042
10	4.10	4.093	003
2	3.91	3.923, 3.917	400, 060
3	3.87	3.869	$\bar{1}$33
2	3.738	3.732	061
10	3.562	3.562, 3.553	113, $\bar{2}$61
18	3.260	3.256	$\bar{1}$14
4	3.227	3.213	261
13	3.117	3.125	203
54	3.077	3.070	004
6	2.822	2.826	370
2	2.780	2.777	114
3	2.695	2.693	$\bar{2}$05
10	2.622	2.625	371
2	2.564	2.563, 2.563	333, $\bar{2}$64
2	2.466	2.460	$\bar{2}$83
2	2.414	2.416	064
7	2.365	2.368, 2.360	372, $\bar{6}$05
1	2.267	2.266	045
2	2.222	2.220	$\bar{2}$84
1	2.144	2.150	$\bar{4}$84
5	2.105	2.110, 2.109, 2.105	373, $\bar{3}$75, 602
1	2.040	2.038	0 10 3
3	1.875	1.875	374
2	1.852	1.853	265
6	1.672	1.673, 1.672, 1.671	375, 484, $\bar{9}$73

TABLE 6. Ring symbols for silicate anions in structures of selected hydrated Mn phyllosilicate minerals

Mineral	Chemical formula	Ring symbol	Fig.	Ref.
Manganpyrosmalite	Fe$_7$Mn$_9$(Si$_{12}$O$_{30}$)(OH)$_{17}$Cl$_3$	$4^3 6^2 12^1$	4a	1
Parsettensite	K$_{7.5}$Mn$_{49}$(Si$_{64.5}$Al$_{7.5}$O$_{168}$)(OH)$_{50}$	$4^3 5^6 6^2 12^2$	4b	2
Varennesite	Na$_8$Mn$_2$(Si$_{10}$O$_{25}$)(Cl$_{0.76}$(OH)$_{1.24}$)(H$_2$O)$_{12}$	$4^2 6^2 10^1$	4c	3
Tamaite (orth.)	CaMn$_6$(Si$_9$AlO$_{24}$)(OH)$_4$·nH$_2$O	$5^1 6^3 7^1$	4d	4
Bannisterite	Ca$_{0.5}$K$_{0.38}$(Mn$_{6.15}$Fe$_{1.43}$Mg$_{1.42}$Zn)((Si$_{14.82}$Al$_{1.18}$)O$_{38}$)(OH)$_8$	$5^2 6^4 7^2$	4e	5
Intersilite	Na$_{5.8}$K$_{0.45}$Mn(Ti$_{0.75}$Nb$_{0.25}$)(Si$_{10}$O$_{24}$)(OH)$_{3.5}$O$_{0.5}$(H$_2$O)$_4$	$5^2 6^2 8^1$	4f	6
Armbrusterite	K$_5$Na$_6$Mn^{3+}Mn$^{2+}_{14}$[Si$_9$O$_{22}$]$_4$(OH)$_{10}$·4H$_2$O	$5^4 6^2 7^2 8^1$	5a	7
Bementite	Mn$_{6.927}$(Si$_6$O$_{15}$)(OH)$_8$	$5^1 6^1 7^1$	5b	8

Note: References: 1 = Kato and Takeuchi 1983; 2 = Eggleton and Guggenheim 1994; 3 = Grice and Gault 1995; 4 = Hughes et al. 2003; 5 = Heaney et al. 1992; 6 = Yamnova et al. 1996; 7 = this work; 8 = Heinrich et al. 1994.
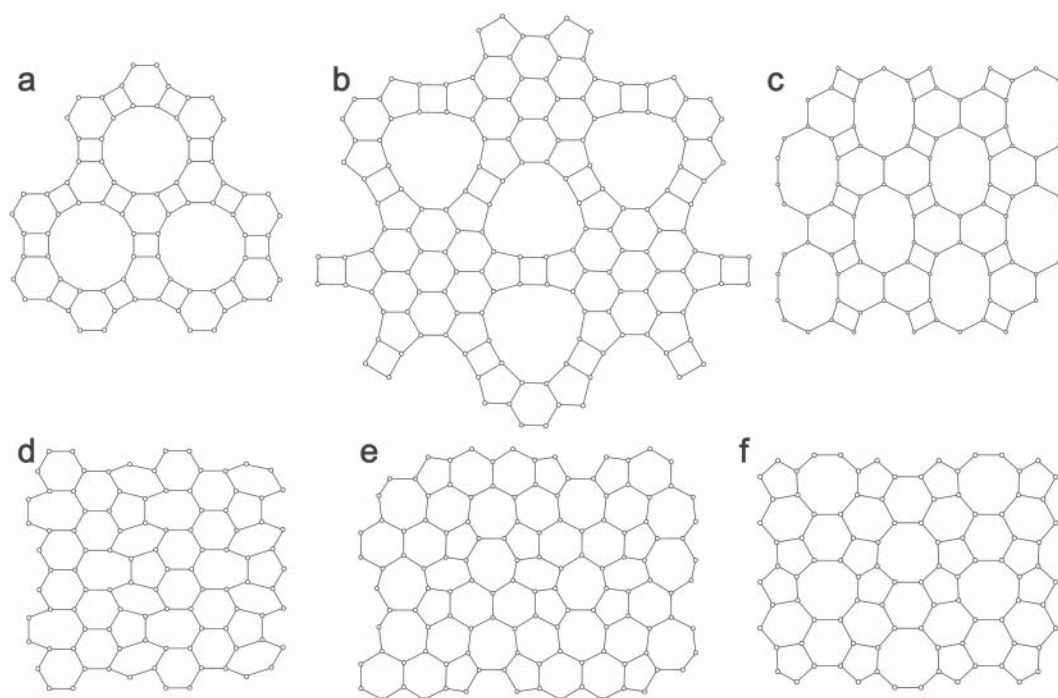
FIGURE 4. Topological diagrams of 2-dimensional silicate anions in hydrophyllosilicates of manganese. See text and Table 6 for details.
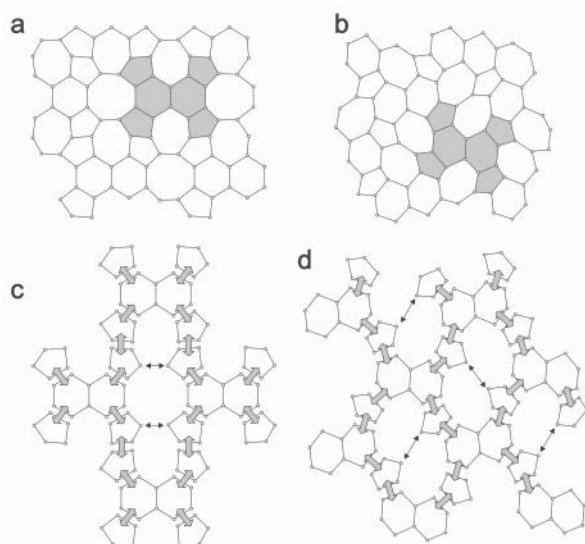

FIGURE 5. Topological diagrams of 2-dimensional silicate anions in armbrusterite (**a**) and bementite (**b**). Selected regions show elements common for both topologies. Graphs shown in **a** and **b** can be constructed by merging 5- and 6-MRs (**c** and **d**, respectively). Thick arrow corresponds to edge-sharing between two rings, whereas thin arrows show places of insertions of new edges between the nodes.

bered rings (6-MRs) (i.e., two hexagonal rings sharing common edge) and 5-membered rings (5-MRs). In both topologies, double 6-MRs share edges with 5-MRs (Figs. 5c and 5d). However, the armbrusterite topology shows twice the number of 5-MRs as in

bementite topology. As a result, 5-MRs in armbrusterite occur in pairs, whereas, in bementite, they are isolated from each other. The topological differences also appear in the linkage of the 6- and 5-MRs: in bementite, linkages polymerize to form 7-MRs, whereas, in armbrusterite, condensation results in formation of 8- and 7-MRs.

As emphasized by Belov (1973) and Liebau (1985), topology and geometry of flexible silicate anions are strongly influenced by cation composition of the chemical system, i.e., size, charge, and chemical hardness of the cations that compensate for the negative charge of the silicate anion. It is noteworthy that the octahedral sheet in armbrusterite consists of three different types of octahedral cations: Na^+ (with average $<Na^+\text{-}O>$ bond length of 2.43–2.47 Å), Mn^{2+} ($<Mn^{2+}\text{-}O> = 2.20$–2.22 Å), and Mn^{3+} ($<Mn^{3+}\text{-}O> = 2.04$ Å). The complexity of the octahedral cation composition is probably responsible for the topology in armbrusterite of 5-, 6-, 7-, and 8-MRs. As far as we know, the only other examples of two-dimensional silicate anions with four different rings are parsettensite (Fig. 4b) and the synthetic compounds of $Na_3Nd(Si_6O_{15})(H_2O)_2$ (Karpov et al. 1977; Haile et al. 1997) and $(Rb, Na)_2(VO)(Si_4O_{10})(H_2O)_x$ (Wang et al. 2002) (see Krivovichev 2005 for topological diagrams).

REFERENCES CITED

Armbruster, T., Oberhaensli, R., Bermanec, V., and Dixon, R. (1993a) Hennomartinite and kornite, two new Mn^{3+} rich silicates from the Wessels Mine, Kalahari, South Africa. Schweizerische Mineralogische und Petrographische Mitteilungen, 73, 349–355.

Armbruster, T., Oberhaensli, R., and Kunz, M. (1993b) Taikanite, $BaSr_2Mn_2^{3+}O_2[Si_4O_{12}]$, from the Wessels Mine, South Africa: a chain silicate related to synthetic $Ca_3Mn_2^{3+}O_2[Si_4O_{12}]$. American Mineralogist, 78, 1088–1095.

Armbruster, T., Kohler, T., Libowitzky, E., Friedrich, A., Miletich, R., Kunz, M., Medenbach, O., and Gutzmer, J. (2001) Structure, compressibility, hydrogen bonding, and dehydration of the tetragonal Mn^{3+} hydrogarnet, henritermierite. American Mineralogist, 86, 147–158.

Armbruster, T., Gnos, E., Dixon, R., Gutzmer, J., Hejny, C., Dobelin, N., and Medenbach, O. (2002) Manganvesuvianite and tweddillite, two new Mn^{3+}-silicate minerals from the Kalahari manganese fields, South Africa. Mineralogical Magazine, 66, 137–150.

Belov, N.V. (1973) Essays in Structural Mineralogy, p. 278. Nauka, Moscow (in Russian).

Brese, N.E. and O'Keeffe, M. (1991) Bond-valence parameters for solids. Acta Crystallographica, B47, 192–197.

Dunitz, J.D., Schomaker, V., and Trueblood, K.N. (1988) Interpretation of atomic displacement parameters from diffraction studies of crystals. Journal of Physical Chemistry, 92, 856–867.

Eggleton, R.A. and Guggenheim, S. (1994) The use of electron optical methods to determine the crystal structure of a modulated phyllosilicate: parsettensite. American Mineralogist, 79, 426–437.

Grice, J.D. and Gault, R.A. (1995) Varennesite, a new species of hydrated Na-Mn silicate with a unique monophyllosilicate structure. Canadian Mineralogist, 33, 1073–1081.

Guggenheim, S. and Eggleton, R.A. (1987) Modulated 2:1 layer silicates: review, systematics, and predictions. American Mineralogist, 72, 724–738.

——— (1988) Crystal chemistry, classification and identification of modulated layer silicates. In S.W. Bailey, Ed., Hydrous Phyllosilicates (Exclusive of Micas), 19, p. 675–725. Reviews in Mineralogy, Mineralogical Society of America, Chantilly, Virginia.

Haile, S.M., Wuensch, B.J., Laudise, R.A., and Maier, J. (1997) Structure of $Na_3NdSi_6O_{15}\cdot2(H_2O)$—a layered silicate with paths for possible fast-ion conduction. Acta Crystallographica, 53, 7–17.

Heaney, P.J., Post, J.E., and Evans, H.T., Jr. (1992) The crystal structure of bannisterite. Clays and Clay Minerals, 40, 129–144.

Heinrich, A.R., Eggleton, R.A., and Guggenheim, S. (1994) Structure and polytypism of bementite, a modulated layer silicate. American Mineralogist, 79, 91–106.

Hughes, J.M., Rakovan, J., Bracco, R., and Gunter, M.E. (2003) The atomic arrangement of the ganophyllite-group modulated silicates as determined from the orthorhombic dimorph of tamaite, with elusive 16.8 Å ganophyllite-group superstructure revealed. American Mineralogist, 88, 1324–1330.

Karpov, O.G., Pushcharovskii, D.Yu., Pobedimskaya, E.A., Burshtein, I.F., and Belov, N.V. (1977) The crystal structure of the rare-earth silicate $NaNdSi_6O_{13}(OH)_2\cdot n(H_2O)$. Soviet Physics Doklady, 22, 464–466.

Kato, T. and Takeuchi, Y. (1983) The pyrosmalite group of minerals I: Structure refinement of manganopyrosmalite. Canadian Mineralogist, 21, 1–6.

Krivovichev, S.V. (2005) Topology of microporous structures. In G. Ferraris and S. Merlino, Eds., Micro- and Mesoporous mineral phases, 57, p. 17–68. Reviews in Mineralogy and Geochemistry, Mineralogical Society of America, Chantilly, Virginia.

Krivovichev, S.V., Yakovenchuk, V.N., Armbruster, T., Pakhomovsky, Ya.A., Weber, H.-P., and Depmeier, W. (2004) Synchrotron X-ray diffraction study of the structure of shafranovskite, $K_2Na_3(Mn,Fe,Na)_4[Si_9(O,OH)_{27}]\cdot nH_2O$, a rare manganese silicate from Kola Peninsula, Russia. American Mineralogist, 89, 1816–1825.

Liebau, F. (1985) Structural Chemistry of Silicates: Structure, Bonding, and Classification, p. 347. Springer-Verlag, Berlin.

Mandarino, J.A. (1981) The Gladstone-Dale relationship: Part IV. The compatibility concept and its application. Canadian Mineralogist, 19, 441–450.

Wang, X., Liu, L., and Jacobson, A.J. (2002) Open-framework and microporous vanadium silicates. Journal of the American Chemical Society, 124, 7812–7820.

Yakovenchuk, V.N., Ivanyuk, G.Yu., Pakhomovsky, Ya.A., and Men'shikov, Yu.P. (2005) Khibiny. Laplandia Minerals, Apatity, p. 467.

Yamnova, N.A., Egorov-Tismenko, Yu.K., and Khomyakov, A.P. (1996) Crystal structure of a new natural (Na,Mn,Ti)-phyllosilicate. Kristallografiya, 41, 257–262 (in Russian).